Research Article

Enhanced Performance of Triboelectric Nanogenerators and Sensors via Cold Spray Particle Deposition

Young Won Kim,* Semih Akin, Huitaek Yun, Shujia Xu, Wenzhuo Wu, and Martin Byung-Guk Jun

Cite This: *ACS Appl. Mater. Interfaces* 2022, 14, 46410−46420

Read Online
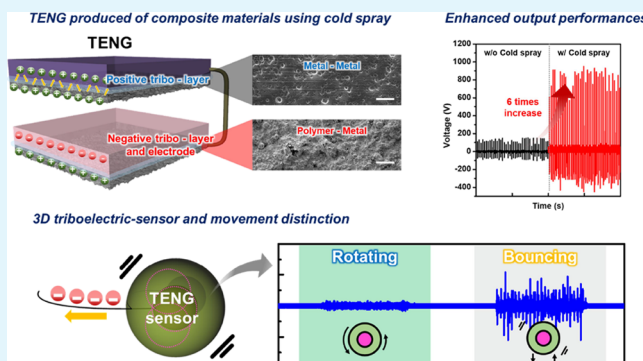
ACCESS | 📊 Metrics & More | 📑 Article Recommendations | Ⓢ Supporting Information

ABSTRACT: In this study, a high-performance triboelectric nanogenerator (TENG) is developed based on cold spray (CS) deposition of composite material layers. Composite layers were fabricated by cold spraying of micron-scale tin (Sn) particles on aluminum (Al) and polytetrafluoroethylene (PTFE) films, which led to improved TENG performance owing to functionalized composite layers as friction layers and electrodes, respectively. As-sprayed tin composite layers not only enhanced the flow of charges by strong adhesion to the target layer but also formed a nano−microstructure on the surface of the layers, thereby increasing the surface area during friction. More importantly, the electricity generation performance was improved more than 6 times as compared to the TENG without CS deposition on it. From parametric studies, the TENG using the cold-sprayed composite layer produced an electrical potential of 1140 V for a simple structure with a 25.4×25.4 mm^2 contact area. We also optimize the geometry and fabrication process of the TENG to increase the manufacturing efficiency while reducing the processing cost. The resultant sprayed layers and structures exhibited sustainable robustness by showing consistent electrical performance after the mechanical adhesion test. The proposed manufacturing approach is also applicable for processing three-dimensional (3D) complex layers owing to the technological convergence of a cold spray gun attached to a robotic arm, which makes possible to fabricate the 3D TENG. To elaborate, a composite layer having the shape of a 3D ball is produced, and the exercise status of the ball is monitored in real-time. The fabricated 3D ball using the TENG transmitted a distinguishable signal in real-time according to the state of the ball. The proposed TENG sensing system can be utilized as a self-powered sensor without the need of a battery, amplifier, and rectifier. The results of this study can potentially provide insights for the practical material design and fabrication of self-powered TENG systems.

KEYWORDS: *triboelectric nanogenerator, triboelectric sensor, cold spray, energy harvesting, self-powered sensor*

1. INTRODUCTION

Energy harvesting systems from the natural environment have been attracting attention for several decades as eco-friendly and infinite alternative energy solutions utilizing wasted energy. As one of the solutions, triboelectric nanogenerators (TENGs), which convert infinite dynamic energy sources (e.g., water wave energy, wind energy, and mechanical energy) into electrical energy, have simple structures and are suitable for generating high-powered energy.[1−5] In addition, because electrostatic potential-based devices based on the TENG have different output electrical signals according to very small contact patterns, many studies have applied the triboelectric system to dynamic movements such as repetitive motion,[6,7] rotation,[8] and vibration[9] to produce customized sensors. TENG is a novel device with lots of advantages including high efficiency, cost-effectiveness, simplicity, and eco-friendliness. It induces the movement of electric charges in such a way that two or more materials with opposite static charges come into contact and separate from each other.[10−12] The induced charge moves to

each electrode on positive and negative parts with opposite electrification rates according to the contact step, and this generated electron flow produces electricity.

There are three main modes of TENGs, which are lateral sliding mode, vertical contact separation mode, and single electrode mode.[13] In general, lateral sliding mode TENGs, in which two triboelectric materials have strong friction in the horizontal direction, generally show higher output performance than other modes. However, lateral sliding mode TENGs have limitations in terms of material selection, high manufacturing cost, complexity of structure, lack of durability, and limited application to rotational motion.[14] On the other hand, the
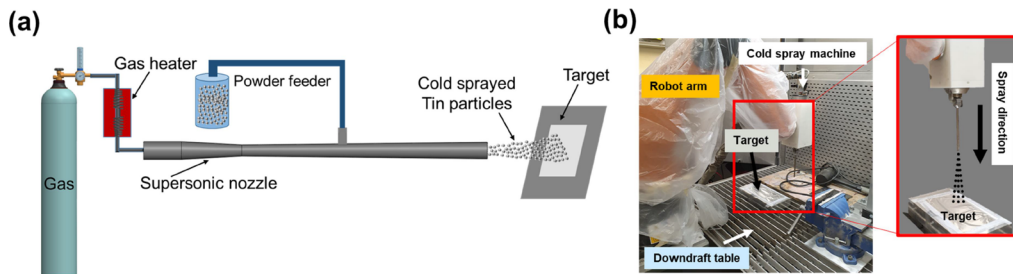
Figure 1. Schematic of the tin (Sn) electrode fabrication process; (a) CS process, (b) experimental setup.

vertical contact mode TENGs are simple structures with various driving methods, numerous material options, and long-operating life, thereby having the potential for actual industrial applications.[15] Also, in the case of the single electrode mode, there are advantages such as a simple device configuration, high intuitivity, and a reduced number of electrodes. As such, the simple single electrode mode is one of the best choices for wearable devices as it makes the fabrication of TENGs simple with minimal design requirements.[16] Past studies related to this mode have improved the output performance by developing electrical negative polarity materials for TENG using embedded nanotubes,[17] graphene,[18] and ceramic materials[19] on a polymer matrix. In particular, recent studies have improved the output performance by fabricating a polymer matrix in the form of nanofibers[20] or using a multilayered matrix for charge trapping.[21] However, constructing actual TENG devices by applying these processes remains challenging because of their process complexity, difficulty for large-scale processing, long manufacturing time, and expensive costs.

To solve these problems from a manufacturing point of view, a cold spray (CS)-based novel manufacturing approach is proposed in the present study as a time and cost-effective alternative to the traditional approaches. To our best knowledge, we are the first to employ the CS particle deposition technique in the production of a TENG. Cold spray, owing to high-speed impingement of particles on target surfaces at low temperatures, is one of the emerging manufacturing techniques that is widely used in high-throughput coating of microparticles on various substrates, including curvilinear 3D shapes. Unlike traditional coating and embedding systems, 3D triboelectric layers can be easily produced through CS, and multi-axis processing capability of CS using a robot arm can expand the application range of the TENG. Moreover, CS is superior in terms of anti-corrosion, wear protection, and scratch resistance against the traditional coating methods.[22] In addition, with the development of related technologies, CS has become a promising additive manufacturing process for state-of-the-art applications requiring improved electrical, mechanical, and chemical properties.[23,24] Besides, CS can produce various composite layers made of polymers and metals while saving time and cost. These layers not only become a single layer of the TENG but also constitute an automatic bonding system for each friction layer and electrode. In general, positive materials of the TENG such as Al, Au, and Cu can be suitable candidates for CS processing because they are easy to be positively charged and electrically conductive because of their excellent electron donor characteristics.[25]

Therefore, the positive materials are used in this study among the many interests of using CS. A composite layer of a positive friction composed of the two positive materials is fabricated using CS. Next, a composite layer, the combination of the negative friction layer and an electrode, is also fabricated by CS.

The produced composite layers show a clear difference in performance based on the charge flow measurements as compared to single (bare) layers. As such, this study is significant to improve not only the performance of friction materials for energy harvesting but also the flow of charge between composite layers and between each layer and electrode. This in turn resulted in an increase in electrical performance, and although only the CS process was added to Al and PTFE films (i.e., known as excellent triboelectric materials), the output voltage was increased more than 6 times as compared to the TENG without CS (i.e., single layer TENG).

We also incorporate the CS system into multi-axis processing using a robot arm to fabricate a 3D composite positive layer inside a tennis ball (i.e., curvilinear surface). This positive layer is applied to the inner side of a tennis ball, designed to form a triboelectric sensor that outputs an electric signal according to the movement. The rubber constituting the inner surface of a tennis ball, relatively easy to obtain electrons, generate a tribo effect by friction with the positive ball, and work as a counterpart material of positive inner ball. The performance of the fabricated 3D tennis ball sensor (i.e., manufactured using triboelectric materials) is also verified through parametric tests by generating different waveforms based on the movement of the tennis ball. The output data of the triboelectric sensor signal is utilized as an indicator of the real-time motion of the tennis ball. Moreover, the 3D tennis ball sensor produced using composite high-efficiency materials is verified by the arch-shaped prototype TENG test. The performance and sensitivity of the sensor are also evaluated under various movement status (i.e., rotating, bouncing) of the ball in real-time.

2. RESULTS AND DISCUSSION

2.1. Composition of TENG and Application Goals of Composite Materials Using the CS Process. TENG is basically an electrical energy generator consisting of a substrate, positive and negative friction materials, and electrode parts. In order to increase the output performance of the TENG, many studies proposed various attempts for each part as follows: Determination of the structure and type of negative materials,[26−28] selection of the structure and type of positive materials,[29,30] and optimization of electrodes.[31,32] When two or more materials with different electrification rates repeatedly contact and separate each other, the charge flows within each part. In order to improve the flow of charge within the layer of the TENG, many studies have been conducted recently by adjusting the thickness within one negative part or by using a composite material.[2,33−35]

However, in the case of the positive part, the selection of materials is limited because the positive friction layer has electrical conductivity and works as a working electrode at the same time. In the current state, there is a critical need for a

manufacturing method that enables bonding dissimilar materials together on the target surface without compromising intrinsic substrates and electrode properties. Here, we employ the CS technique as a potential candidate to address the aforementioned manufacturing approaches in a manner that positive and negative layer high-performance electrodes can be produced to improve the performance of the TENG.

Cold spray (CS) is an emerging technology for solid-state rapid deposition of microscale metal particles on a target surface as a result of high-velocity impact.[36] In the CS deposition process, as depicted in Figure 1a, feedstock microscale (typically <50 μm) metal particles are accelerated to high velocities (e.g., 300−1200 m/s) through a converging−diverging nozzle using compressed gases (e.g., air, nitrogen, and helium) followed by impact/impingement onto a target surface.[37] When the particles impact the surface, particles' kinetic energy disperses onto the surface, resulting in strong interfacial adhesion due to the high-impact velocity of particles.[38,39]

In the present study, we use a low-pressure CS machine system (Rus Sonic Technology, Inc.) to fabricate working electrodes for the triboelectric nanogenerator. The CS nozzle was mounted on a 6-axis robot arm (Kuka KR AGILUS) to precisely control the deposition process (see Figure 1b). Micron-scale tin (Sn) particles having a spherical morphology (Centerline Ltd) were used as the feedstock material. Tin particles are in the size range of −45 to +5 μm with an average diameter of 17 μm.[40] In general, tin, one of the coating materials in CS, has good corrosion resistance; therefore, it prevents the change of target metals during the plating process. As such, the tin particles were used in the present study as the functional coating material owing to its positive charge density in triboelectric applications.[41] Cold spraying experiments were conducted using the operational process parameters listed in Table 1. The robot arm was pre-programmed for spray patterning, and CS deposition was carried out under vacuum- and mask-free conditions.

Table 1. Operating Parameters of the Cold Spray Process

process parameters	value
working gas	air
driving gas pressure (MPa)	0.7
driving gas temperature (°C)	80
gas flow rate (m³ h⁻¹)	34
powder flow rate (g s⁻¹)	0.15
nozzle transverse speed (mm s⁻¹)	50
nozzle stand-off distance (mm)	30

2.2. Effect of CS on TENG Performance. In order to check the effect of CS particle deposition on the TENG, the generally designed arch-shaped TENG structure was fabricated, as shown in Figure 2a.[27,35] In this study, the TENG fabricated using PI (Polyimide) film as a substrate has a simple structure with the advantage of being able to control the distance between the two friction layers and automatically separate after contact. This PI-type TENG includes a substrate, the combination of two parts: a positive part including the positive layer and a negative part including the negative layer and the electrode, and a wire connected to each part. Because the positive layer uses Al that can act as an electrode by itself, the positive part does not include an additional electrode. Figure 2b shows the schematic diagram of the cross-section view of the PI arch-shaped TENG. When input pressure is applied to the TENG in the vertical direction,

the positive and negative layers come closer and in contact. Conversely, when the pressure is released, the two layers are separated from each other because of the elastic force of the PI substrate. At this time, the flow of charge forms as shown in Figure 2c. The main focus of the present study is to improve the amount of positive charge in the positive layer and the flow of charge at the interface between the negative layer and the electrode. The contribution of this study is that the enhanced positive composite layer can be quickly and efficiently fabricated using the CS coating technique. Tin (Sn) coating can be also produced as a uniformly dense layer through CS coating technology and can be stably deposited on various materials.[42,43] In the experiments, the CS-coated Sn layer was variously applied to increase the performance of the TENG.

Figure 3a shows the surface scanning electron microscopy (SEM) images of bare Sn film, Al film, and PTFE film. A bare Sn film is used for comparison with as-cold sprayed tin particles, visualizing the differences according to the shape of tin, and a single PTFE and Al film can be a composite material with sprayed tin. These single films and composite films are the materials constituting the friction layer to determine the effect of CS on the TENG performance. The state of tin particles before and after performing CS on the target is shown as an SEM image in Figure 3b. CS results show that tin particles are embedded on the PTFE and Al surfaces; therefore, the surface roughness is increased. Specifically, the surface roughness (R_a) value of the PTFE (i.e., initially was 0.673 μm) increased more than 10 times to 7.63 μm after CS, and the Al film (0.231 μm) showed a similarly large increase to 2.90 μm after the CS process, as shown in Figure S1. Even in the case of the Al−Tin composite layer, the opposite side of the spray-coated layer had a value of 2.87 μm, which means that the surface roughness was increased on both sides. Increased surface roughness helps form an increased dipole moment between the friction layers, generate more triboelectric charges, and improve capacitance and effective dielectric constant during the contact.[44,45] In particular, in the case of the deformable PTFE polymer, it can be seen from Figure 3c that the particles impinge into the surface and form a thick sprayed Sn layer. For the Al layer, it can be confirmed that a thin Sn layer is formed on a relatively thin substrate (see Figure 3c). As a result of thickness measurement, the Sn layer with a thickness of 110 μm was fabricated on the PTFE film and on Al with a thickness of 0.02 μm. To make it clear whether those Sn layers are sprayed on the target layer well, the SEM image and energy-dispersive X-ray spectroscopy (EDX) mapping of the Sn layer are shown in S2. These figures prove that Sn powder was well deposited on the target substrate. The Sn-PTFE composite layer is made of a heterogeneous material composed of metal and polymer and is a single combined layer, but PTFE can act as a negative material and the sprayed Sn layer can act as an electrode. These two materials are very densely and strongly bonded through the CS process, and at the same time, each layer has its own role. As it is not yet known what kind of synergistic effect the composite layer made with CS exerts on the output performance of the TENG, we produced the TENG of the arch structure presented in Figure 2c with various combinations of materials using CS for the confirmation. Figure 4 shows a diagram of the simple structure of four types of TENGs manufactured under the same conditions and the TENG output results during hand-tapping. The charge induced on the surface of the negative material at the approach of the two layers flows in turn to the positive material through the electrodes when the friction layers are separated. Because the negative layer and the
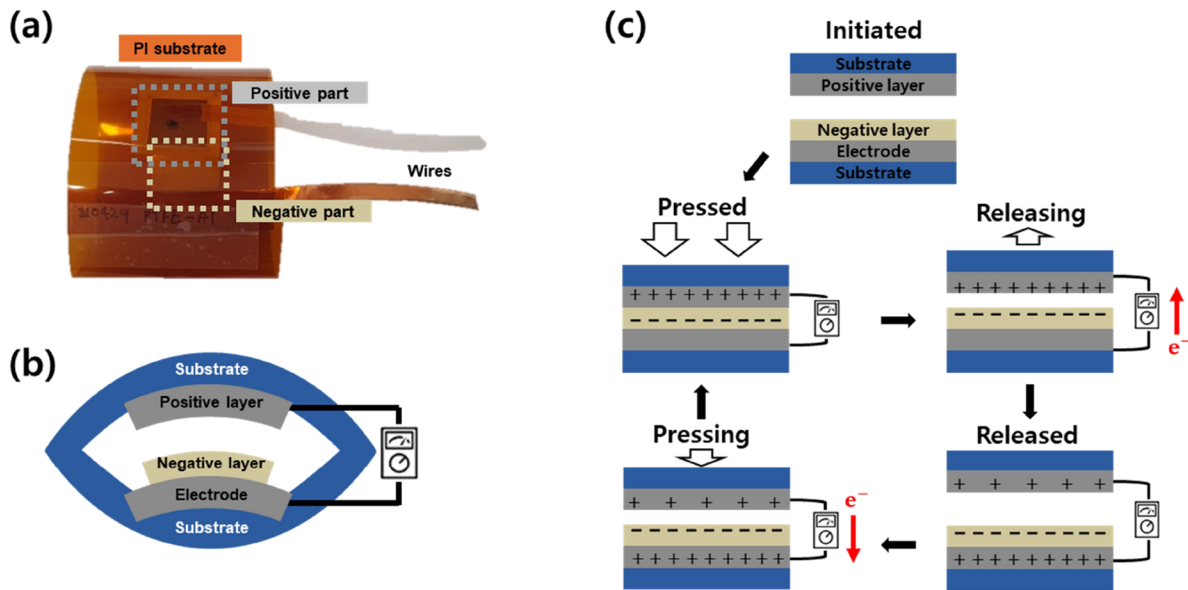
Figure 2. (a) Photograph of the actual device and (b) schematic of a cross-sectional view of arch type TENG. (c) Schematic illustration of charge transfer as the device operates of vertical contact and separate mode TENG.
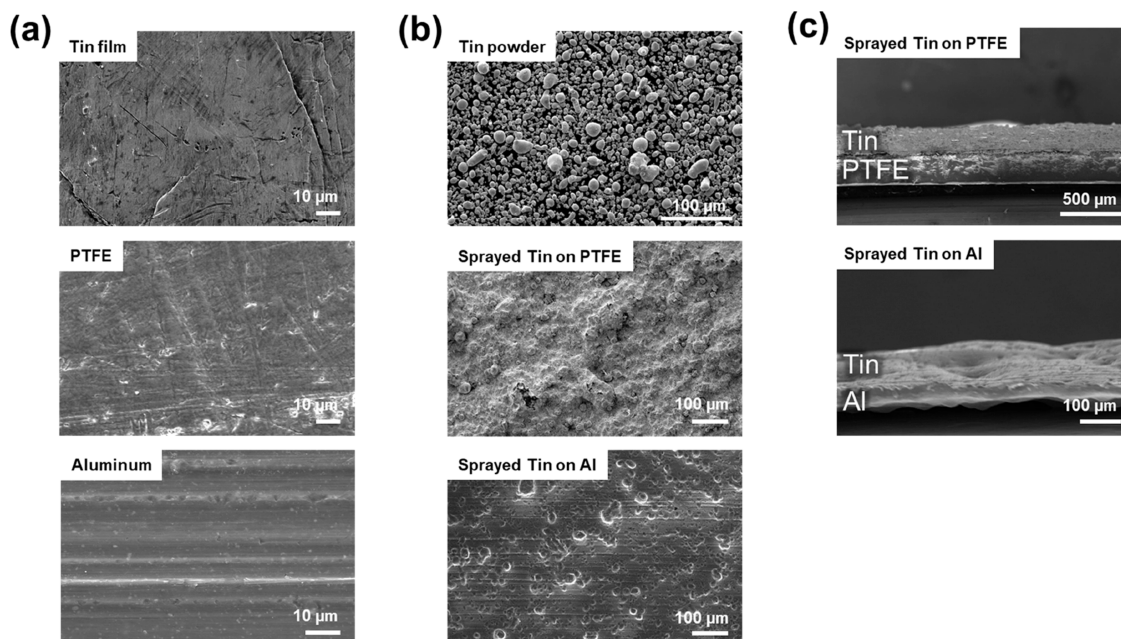
Figure 3. (a) Surface SEM images of the bare Sn film, bare PTFE film, and bare aluminum film. (b) Surface morphology of Sn powders (upper panel), as-cold-sprayed Sn layer on PTFE (middle panel), and as-cold-sprayed Al film (bottom panel). (c) Cross-sectional SEM images of tin-PTFE and tin-PTFE after CS.

electrode are different materials, there is a risk of charge loss if the two surfaces are not in perfect contact. CS is one of the solutions for strongly and densely bonding the negative layer and the electrode. Negative layers of all PI arch-type TENGs were made of PTFE, and all conditions were the same except for the positive layer and electrode material to analyze the effect in this experiment. In Figure 4a, the TENG was composed of a positive layer and electrode using tin film and generated an average output of 94($\pm$8) V. In Figure 4b, the TENG uses tin cold sprayed on PTFE as a positive layer, and the output result is reduced by about 30% to 65($\pm$5) V. The only difference between these two experiments is that the tin powder layer coated on PTFE used is thinner than the tin film as a positive

layer. According to the formula related to the electric fields in the two tribo-material layers and in the gap, the triboelectric effect can be relatively reduced because of the use of a positive layer with a low thickness.[46] However, Figure 4c shows that when cold-sprayed Sn is used as an electrode, the output is 171($\pm$21) V, and the performance is increased by 180% compared to that shown in Figure 4a, where Sn film is used as an electrode. In TENG's electrode, thickness has little effect on performance; however, electrical conductivity and adhesion to negative material are the most important factors.[47,48]

The sprayed Sn layer on the PTFE exhibited an electrical conductivity of 2.9×10^5 S/m, without a significant change in resistance after 50 Scotch-tape peeling tests (Figure 6a), which
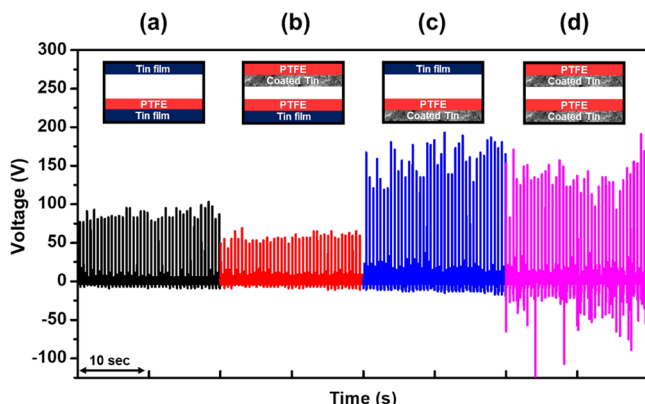
Figure 4. Triboelectric output voltage using (a) bare Sn film and bare tin film, (b) coated (as-cold-sprayed) Sn film and bare Sn film, (c) bare Sn film and as-cold spray coated Sn film, and (d) coated Sn film as the positive material and coated Sn film as an electrode.

Figure 5. Triboelectric output voltage using (a) Al film and Al film, (b) Al–Sn and Al film, (c) Al film and Al–Sn, and (d) Al–Sn and Al–Sn as a positive material and an electrode.

also confirms the adhesion between the as-cold-sprayed Sn layer and the substrate. The low electrical conductivity of the electrode and poor bonding with the negative layer cause partial short circuit or resistance when charge flows, which degrades the performance of TENG. Although the same Sn material with the same electrical conductivity was used for the electrode of the TENG, the CS process improved the bonding issue, thereby the voltage output significantly improved. This means that the electrode coating using the CS process on the negative layer of the TENG can solve the problem of poor surface bonding that hinders the flow of charge. Figure 4d is a TENG in which the tin–PTFE layer produced using the same process is applied to the positive and negative parts at the same time, and CS Sn coating was used as a positive layer but also as an electrode, so that it increased the output voltage as 178($\pm$24) V. The TENG in Figure 4d shows unevenness of the output compared to the TENG, as shown in Figure 4c; however, in terms of process efficiency, it has the advantage of shortening the manufacturing time and process steps because all active layers of the TENG are completely composed of using the same composite layer twice. Additionally, the CS process is a cost-effective process requiring a smaller amount of feedstock Sn powders as compared to bare Sn films. These results reveal that even though the same material with the same dielectric constant and electrical conductivity is used, the performance of the TENG and the efficiency of manufacturing can be increased by the CS process, which can eventually lead to large-scale deployment of the high-performance TENG. In addition, the trend of these different voltage output results was also observed in the current measurement results, confirming that CS can affect the current movement (Figure S3).

In the next experiment, CS was also applied to an Al film to be a positive material as in most of TENG-related studies. Al not only increases the surface area by increasing the surface roughness through Sn coating but also induces an alteration in the dielectric constant or capacitance at the interface where different metals are bonded. This approach using the CS process greatly affects the output performance of the TENG. The experimental results of the four different TENGs in Figure 5 show that Al used as the positive layer or electrode of the TENG was replaced with Al–tin, and the role of the composite layer was accurately drawn. As shown in Figure 5a, an average output voltage of 192($\pm$36) V for each tapping was obtained by employing Al as the positive layer, PTFE as the negative layer,
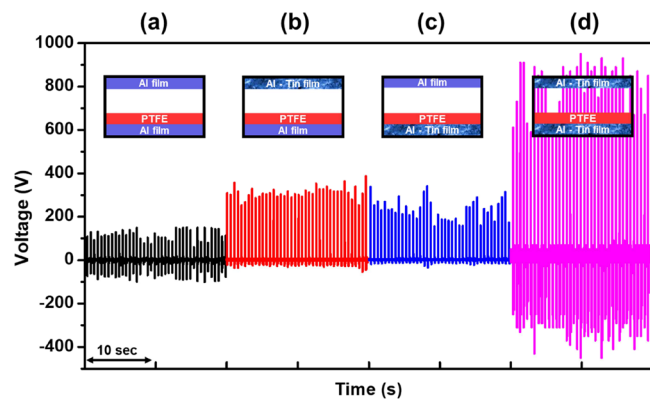
and Al as the electrode, respectively. When the positive layer of TENG of the same structure was replaced with the Al–Sn layer and the electrode was replaced with the Al–Sn layer, the performance increased to 337($\pm$26) V (Figure 5b) and 247($\pm$39) V (Figure 5c), respectively. These two results indicate two different meanings: (1) the Al–Tin composite material shows higher performance than Al as a positive friction material; therefore, it can replace the Al film used in many existing studies and applications; (2) it is confirmed that the Al–Sn layer shows better performance compared to the conventional Al film as an electrode. Considering these findings, we fabricated a novel type of TENG, as shown in Figure 5d, which showed a sharp increase in the average output electrical performance to 1141($\pm$102) V. The performance of the TENG increased dramatically compared to the sum of the performance increases through the improvement of each positive material and electrode material, and this was also confirmed by the current measurement results (Figure S4). This means that the combination and synergy of the positive layer and electrode as well as the negative layer should be considered when designing TENG. It is confirmed that the Al–Tin composite layer has an excellent electrical conductivity of 1.41×10^6 S/m firmly adhered to each other to prevent deterioration in properties even after the peeling test (see Figure 6b).

To investigate the multidirectional performance of the device with the optimal combination (Figure 5d) Al–tin and Al–tin as
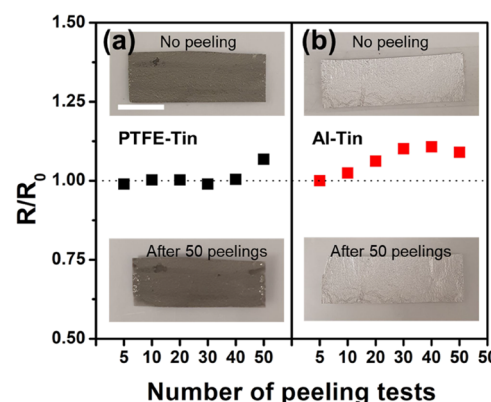
Figure 6. Relative resistance of Sn sprayed on (a) PTFE and (b) Al film according to the peeling test, and specimens before and after the peeling test (scale bar: 10 mm).
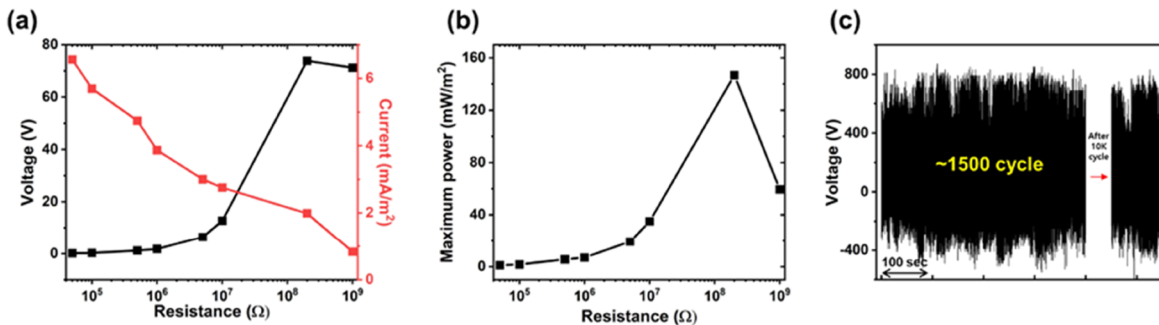
Figure 7. All about Figure 5d, in which TENG showed the most optimal performance. (a) Output voltage and current dependencies for different loading resistances. (b) Relationship between output power and external loading resistance. (c) Durability test performed via 1500 cycles and measurement results after 10 K cycles.
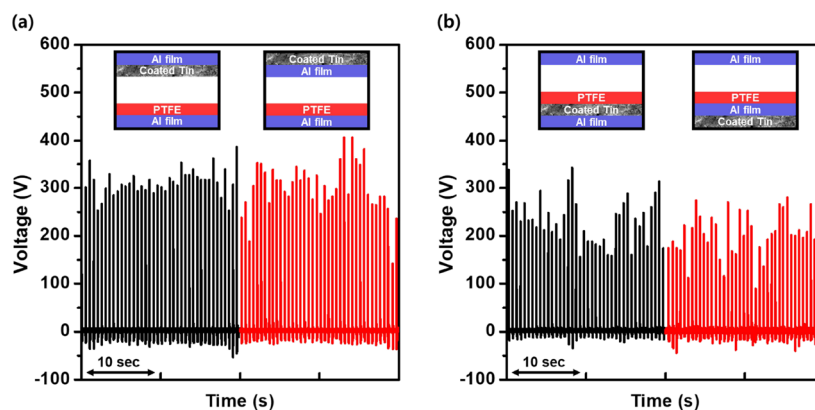
Figure 8. Comparison of triboelectric output voltage according to the direction of the composite material as (a) a positive layer and (b) an electrode.
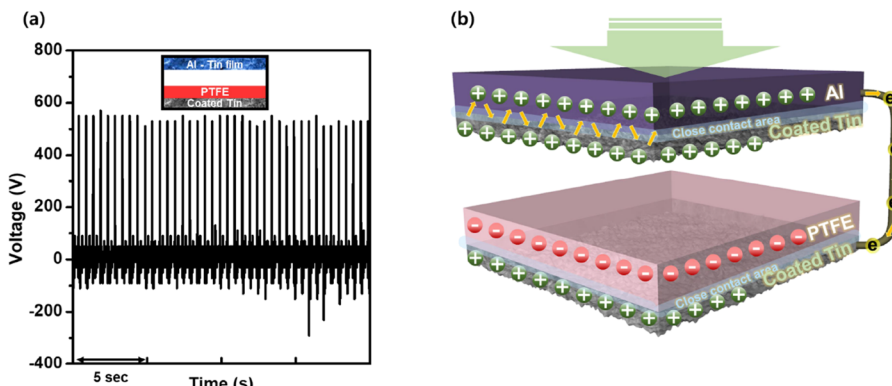
Figure 9. (a) Triboelectric output voltage using Al−Sn and CS-coated Sn. (b) Charge transfer through the composite materials.

a positive material and an electrode, we measured voltage, current, and power density while loading external resistors, as shown in Figure 7a, b. The voltage and power density were the highest at 200 M ohm, and the values were 74 V and 147 mW/m^2, respectively. The voltage drop was caused by the external resistance, and voltage difference was caused by the internal resistance of the device itself. Figure 7c illustrates that there was no performance degradation during repeated contacting and separating via 1500 cycles and after 10 K cycles, with the peak-to-peak voltage output sustained at about 1100 V.

In addition, using the same Al−Sn layer twice for the positive layer and electrode of TENG makes it possible to efficiently save manufacturing time and costs. Although this experiment revealed that the Al−Tin composite layer affects the TENG performance, it remains to be determined whether the material

properties of the layer itself or the composite structure are the reason. Therefore, we uncovered factors affecting the performance of TENG by changing the orientation of the Al−tin composite layer. Figure 8a demonstrates the test result by changing only the direction of the Al−Sn layer of TENG. The type in which the tin coated through CS is in contact with the negative layer generated a voltage of 337 V, and the type in which the opposite side of Al is in contact with the negative layer is 324 V (see Figure 8b). This result indicates that there is no significant difference between Al and tin as a material of the surface contact layer, and the increased surface roughness on both sides of Al−tin due to CS coating affects TENG performance equally. This is likely attributed to the high ductility of the Al foil. To elaborate, when the CS is applied to one side, deformation occurs not only on the target side but also

on the opposite side, which increases the surface roughness. The fundamental reason behind this phenomenon is that the Al−Tin composite as a positive layer affects the output result and the structural combination of these two materials. The Al−Tin composite layer applied as an electrode layer also showed no significant difference with an average of 247 and 220 V of TENG performance, respectively, even if the direction was changed as shown in Figure 8b. Also, distinguishing difference was not observed in the current measurement results, as shown in Figure S5. Because the surface adhesion between the electrode layer and the negative layer is related to the flow of charge, it can significantly affect the performance of the TENG. However, the output results with no significant difference indicate that there is no noticeable difference in adhesion performance between the PTFE surface and the as-cold-sprayed Al or Sn surface.

We also produced the TENG using an Al−tin composite layer as a positive layer and a PTFE-coated Sn layer as a negative layer and electrode based on the results of previous experiments (Figure 9a). At this time, the output increased dramatically to 653 V, which originated from two reasons. As demonstrated in Figure 9b, sprayed tin powder added to Al in the positive part can maximize the triboelectric effect by increasing the surface area as well as the amount of positive charge by itself.[49,50] In addition, the tin particles adhered to the negative layer, PTFE, is a highly conductive metal by itself and is in close contact with the negative layer to prevent loss of charge by increasing the TENG's performance. This TENG, produced using the synergistic effect of two parts with the same CS process, is also promising in terms of improved electrical performance and manufacturing (processing) simplicity.

2.3. 3D (Tennis Ball-Type) TENGs. Because TENG is a simple structure and can be fabricated with simple operation, the range of application is very wide to be applied to any place where dynamic movement occurs. When two substances with a potential difference repeat contact and separation, the TENG generates electrical energy, which makes the TENG not only an energy-harvesting device but also a sensor by analyzing the output signal. When any movement (e.g., vertical or horizontal movement, vibration, torsion, or rotation) drives the TENG as an input, the output signal also changes accordingly; therefore, it can be applied as a sensor to any moving objects. Luo et al. developed a triboelectric sensor for a smart ping-pong table and built a ball judgment system, and Shi et al. demonstrated a 3D spherical-shaped water-based triboelectric nanogenerator device by utilizing the system to harvest wave energy.[51,52]

Besides their advantages, there are still countless devices that use dynamic energy in real life, and more research on triboelectric sensors using them is highly demanded. To this end, in this study, we propose a 3D TENG application manufactured inside a tennis ball that can be easily encountered in daily life and can be utilized as the TENG by generating dynamic kinetic energy. The ultimate goal is to develop a ball-type TENG that generates electric energy whenever the tennis ball moves by inserting an inner ball composed of a positive part into the tennis ball. We conducted a case study to determine which materials are suitable for the ball-type TENG. As shown in Figure 10a, the tennis ball is made of felt by mixing wool and nylon in the outer substrate, and the inner core is composed of natural rubber. When the inner ball is inserted, the surface of the inner ball can repeatly contact and separate from the surface of natural rubber. As such, when in movement, we can use this contact and separation as input dynamic energy for a new type of TENG. Here, we used natural rubber as a negative material
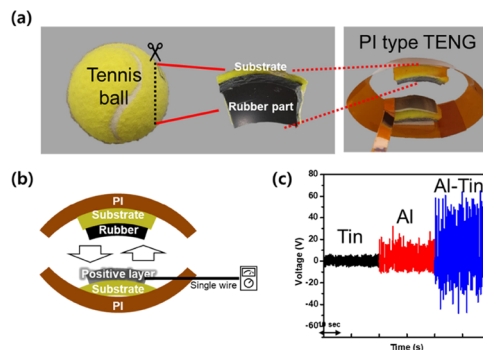
Figure 10. (a) Schematic illustration of overall procedures for the fabrication of arch-type TENG for the parametric test and (b) cross-sectional view. (c) Triboelectric output voltage using Sn, Al, and Al−Sn as a positive layer.

because it was reported as one of the triboelectric materials with electrical negative polarity like PTFE in previous experiments.[53,54] Therefore, to find the optimal positive material when using rubber as a negative material for ball-type TENG, a parametric study was performed by producing TENGs using PI film as a substrate, as shown on the right side of Figure 10a. One of the cut-tennis ball specimens was attached to the top of the PI-type TENG so that the rubber could act as a negative layer. The other cut specimen was attached under the positive layer and fixed at the bottom of the PI-type TENG to have the curved surface of the tennis ball (Figure 10b) for the parametric case study. Because it is not easy to peel off the tennis ball layer and attach an electrode between rubber and felt, a single-electrode mode that requires fewer electrodes and has a simpler structure was applied.

In order to propose the best selection of the positive material, which is a parameter in this experiment, all structures and materials except for the positive layer were kept constant during the experiment. The positive layer consists of three types, which are cold-sprayed tin, Al film, and Al−tin film, with the output results of each 9.4, 26.7, and 77.5 V, respectively. Al−Sn showed the highest output performance as a relative polarization material of rubber as a negative material. This result underlines that Al−tin composite material is more suitable to be used as a positive material as a counterpart to rubber in single-electrode mode than Al and as-cold sprayed Sn. Therefore, our proposed Al−Sn composite material can be a high-efficient composite material that constitutes a positive part not only in the vertical contact-separation mode and single electrode mode but also in the lateral sliding mode and freestanding triboelectric layer mode as verified in this study.

In addition, the Al−Sn composite material can be fabricated in various shapes to the extent that it constitutes the outer layer of the 3D ball. Based on the results of the parametric study, we used sprayed tin, Al, and Al−Sn as substrate materials for positive layers surrounding a PTFE ball having a diameter of 25.4 mm. As shown in Figure 11a, the inner core wall of the tennis ball is made of rubber as a negative material of this ball-type TENG, and it is connected to the positive layer coated on the outer surface of the inserted inner ball through the connected wire while repeating contact and separation. The electric signal generated by the flowing charges is transmitted to an external measuring device. In addition, the CS gun configured by a six-axis robot arm can move freely according to the shape of the target, enabling to coating not only the 2D film but also the front surface of the 3D-shaped target substrate. As such, three
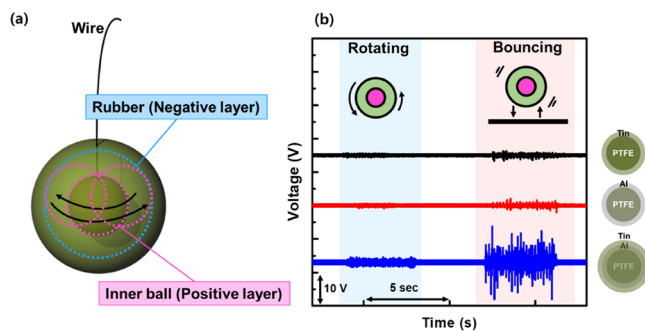
Figure 11. (a) Schematic illustration of tennis ball-type TENG with the single electrode type and (b) triboelectric output voltage using tin, Al, and Al−Sn as a positive layer under various motions of the ball.

types of positive inner balls (i.e., manufactured using multi-axis CS patterning) were inserted into each tennis ball, and a voltage signal was measured from the ball-type TENG driven by the movement of the tennis ball (see Figure 11b). In order to check whether the different movements of the tennis ball can be distinguished, the state of the ball was given two movement conditions: (1) rotating and (2) bouncing, and each movement cycle occurred 5 times per second. The voltage signal output from different positive layers in the tennis ball-type TENGs was distinguished by the difference between rotating and bouncing conditions through its waveform and size. To elaborate when the positive layer is composed of an Al−tin composite material, the signal amplitude was significantly improved under the rotating and bouncing conditions compared to the single material. This means that more power can be harvested from an energy-harvesting point of view, and more precise motion measurement is possible from the aspect of the sensor's performance. Above all, each signal output has 5 peaks per second due to movements of 5 times per second, which proves the output signal (i.e., the electrical energy) generated by the movement of the tennis ball. This result suggests that the proposed ball-type TENG appropriately performs as a triboelectric sensor that can even detect minor frequency changes of the ball in real-time.

We also conducted an economical cost analysis of the proposed manufacturing approach. Table 2 lists the cost of each material used in the fabrication of a TENG device. Each arch-type TENG device costs about $3.6 while a tennis ball-type TENG costs $5.7. Even excluding PI or ball substrates, core

material costs of each TENGs corresponds to $0.276 and $0.141. These high-efficiency core materials can be applied to various substrates and their cost can be even cheaper depending on the type of the substrate. Taken together, we envision that the triboelectric layers with a simple structure and low footprint proposed in this study can have promising potential in wearable electronic devices with self-powered functions in the future.

3. CONCLUSIONS

We proposed a TENG with enhanced performance and demonstrated a 3D spherical shape self-powered triboelectric sensor based on CS metallic powder composite material deposition. Cold-sprayed composite materials have been proven to have superior triboelectric performance compared to single materials owing to increased surface roughness, electrical conductivity, stability, and high adhesion performance. In particular, the new composite material achieved using the CS technique can help the rapid commercialization of TENG owing to inherent advantages of CS including process simplicity, manufacturing efficiency, and low cost as compared to traditional manufacturing methods of TENG. In addition, a TENG applied to the inner side of a tennis ball showed the potential for practical use in a manner that CS-based composite material can be applied to any type of the 3D shape. Collectively, the technical advancements represented in this study can enable many further practical applications for high-performance triboelectric systems, especially for real exercise equipment with the 3D curvilinear geometry.

4. EXPERIMENTAL METHOD

4.1. Fabrication Method of TENGs with Composite Layers on the Spherical Surface. In order to investigate the effect of each friction layer and electrode on the performance of the TENG, the arch-shaped substrate, which is generally used for vertical contact and separation mode TENG, was produced using PI film.[55−57] The substrate, which has spacer and elasticity itself, was made by folding a 1.3 mm thick, 63.5 mm wide, 200 mm long rectangular PI film in a round shape. It is designed to contact each other when input pressure occurs. A 15 μm thick Al film was used as one of the materials constituting the positive layer and the electrode, and the thickness of the polytetrafluoroethylene (PTFE) film as the negative layer was 0.254 mm. Because all layers are 25.4 mm wide by 25.4 mm long, the contact area where the triboelectric effect occurs is 645 mm^2. A low-pressure CS machine (Rus Sonic Technology, Inc.) was used to deposit tin (Sn) metallic particles on the target surface. CS was applied to the surface of

Table 2. Cost of Raw Material To Produce an Arch-Type TENG and a Tennis Ball-Type TENG

items	specification	retail price (USD)	usage amount	usage cost (USD)
1. arch-type TENG				
McMaster PI film	0.09 m^2	29.96	0.01 m^2	3.3
McMaster PTFE film	0.27 m^2	42.48	0.00065 m^2	0.1
Reynolds aluminum foil	91.44 m^2	166	0.00065 m^2	0.001
SST Tin powder S6001	454 g	39	0.059 mg (0.05 mg on PTFE) (0.009 mg on Al)	0.005
McMaster copper tape electrode	16.5 m	19.96	0.1 m	0.1
McMaster mounting foam tape	250 pcs	8.41	2 pcs	0.07
total				**3.576 0.276 (w/o substrate)**
2. tennis ball-type TENG				
Penn tennis ball	3 ea.	2.37	1 ea.	0.79
McMaster PTFE inner ball	1 ea.	4.73	1 ea.	4.73
Reynolds aluminum foil	91.44 m^2	166	0.008 m^2	0.01
SST Tin powder S6001	454 g	39	0.11 mg	0.001
McMaster solid wire electrode	7.62 m	10.21	0.1 m	0.13
total				**5.661 0.141 (w/o substrate)**

PTFE film and Al film at the operating conditions listed in Table 1. CS was also applied to the surface of the PTFE ball followed by wrapping the as-cold sprayed layer with aluminum (Al) foil to produce the inner ball as a positive material in the configuration of the spherical surface. The CS nozzle was attached to a six-axis robot arm (Kuka KR AGILUS) to precisely control the deposition process. The robotic arm was pre-programmed to coat 3D spheres at ambient conditions under mask-free conditions. Sn powders having a size range in 40−50 μm with the spherical morphology was cold sprayed on the target surface.

Through a parametric study before the application of the tennis ball, a spherical prototype TENG was fabricated with an arch-shaped PI film substrate. A portion of a tennis ball was cut out and fixed to one side so that a layer of rubber could constitute the negative part of the prototype TENG. On the other side, various types of positive layers were fixed on the piece of tennis ball to match the curvature with the rubber of the negative part. The inner ball made of 25.4 mm diameter PTFE material was wrapped with a positive layer and the wire was connected to act as a positive ball layer. When adding a positive layer to the PTFE ball, CS was applied directly to the ball, or wrapped with an Al film, or CS was added after wrapping. The produced positive ball layer was inserted into a tennis ball with a 70 mm diameter to compose a spherical triboelectric sensor.

4.2. Electrical Conductivity, Adhesion Force, and Surface Roughness Test of CS Tin Coating. The equation $\rho = R \times A/L$ was used to calculate the conductivity, where ρ is the electrical resistivity, R is the resistance, A is the cross-sectional area of the circuit, and L is the circuit length.[58] All specimens for electrical conductivity measurement have a width of 0.1×10^{-3} m and a length of 0.3×10^{-3} m. Tin-sprayed PTFE and tin-sprayed Al surfaces showed resistances of 0.091 and 0.106 Ω, respectively, and thicknesses of 113 and 20.1 μm. Also, electrical conductivity, σ, is calculated as the inverse of resistivity. At this time, the average resistance and thickness were measured by measuring five different points using a digital multimeter (34401A, Agilent Technologies, USA) and a digital micrometer (REXBETI).

The peeling test (i.e., a method to measure the adhesion force between the coated tin powder layer and the substrate) was conducted to characterize the adhesion strength of the resulting CS coatings. The peeling test was applied while fixing the specimen on a table and repeatedly attaching and peeling 3M scotch tape.[59] The relative resistance ($R\backslash R_o$) change was then recorded for each peeling test to plot the results in Figure 6.

The average surface roughness value (arithmetic mean roughness (R_a)) of the as-cold-sprayed composite layers were measured by repeating measurements five times using a surface roughness tester (SJ-210, Mitutoyo, Japan) on the specimens fixed on a glass substrate.

4.3. Evaluation of Output (Voltage Generation) Performance. To evaluate the output performance, all as-fabricated TENGs were connected to an oscilloscope (DPO2024B, Tektronix, USA), and the open circuit voltage was measured. In the arch type TENG, flat copper tape with 5 mm wide and 76 μm thickness was connected to each electrode and tested for stable electrical connection via 2 hand tappings per second. In the case of the tennis ball triboelectric sensor, a 0.254 mm diameter copper wire was connected only to the positive ball layer, and the oscilloscope measured the output of the single electrode mode. At this time, five revolutions per second in the rolling mode and five input motions per second in the bouncing mode were applied.

ASSOCIATED CONTENT

ⓈI Supporting Information

The Supporting Information is available free of charge at https://pubs.acs.org/doi/10.1021/acsami.2c09367.

> Surface roughness result before and after CS; SEM image and EDX mapping of the cold-sprayed Sn layer; triboelectric direct current; and comparison of tribo-electric direct current according to the direction of the composite material (PDF)
>
> Peeling test (PTFE−tin) (MP4)
>
> Pelling test (Al−tin) (MP4)

Tennis ball-type TENG sensor test (MP4)

AUTHOR INFORMATION

Corresponding Author

Young Won Kim − *School of Mechanical Engineering, Purdue University, West Lafayette, Indiana 47906, United States;* ⓞ orcid.org/0000-0001-7345-9486; Phone: +1 (765) 775-0550; Email: kim3584@purdue.edu

Authors

Semih Akin − *School of Mechanical Engineering, Purdue University, West Lafayette, Indiana 47906, United States*

Huitaek Yun − *Indiana Manufacturing Competitiveness Center (IN-MaC), Purdue University, West Lafayette, Indiana 47906, United States*

Shujia Xu − *School of Industrial Engineering, Purdue University, West Lafayette, Indiana 47906, United States;* ⓞ orcid.org/0000-0002-3173-8249

Wenzhuo Wu − *School of Industrial Engineering, Purdue University, West Lafayette, Indiana 47906, United States;* ⓞ orcid.org/0000-0003-0362-6650

Martin Byung-Guk Jun − *School of Mechanical Engineering and Indiana Manufacturing Competitiveness Center (IN-MaC), Purdue University, West Lafayette, Indiana 47906, United States;* ⓞ orcid.org/0000-0002-0512-7209

Complete contact information is available at:
https://pubs.acs.org/10.1021/acsami.2c09367

Notes

The authors declare no competing financial interest.

REFERENCES

(1) Kanik, M.; Say, M. G.; Daglar, B.; Yavuz, A. F.; Dolas, M. H.; El-Ashry, M. M.; Bayindir, M. A Motion- and Sound-Activated, 3D-Printed, Chalcogenide-Based Triboelectric Nanogenerator. *Adv. Mater.* **2015**, *27*, 2367−2376.

(2) Kim, D. W.; Lee, J. H.; You, I.; Kim, J. K.; Jeong, U. Adding a Stretchable Deep-Trap Interlayer for High-Performance Stretchable Triboelectric Nanogenerators. *Nano Energy* **2018**, *50*, 192−200.

(3) Khandelwal, G.; Minocha, T.; Yadav, S. K.; Chandrasekhar, A.; Maria Joseph Raj, N. P.; Gupta, S. C.; Kim, S.-J. All Edible Materials Derived Biocompatible and Biodegradable Triboelectric Nanogenerator. *Nano Energy* **2019**, *65*, No. 104016.

(4) Zhang, Q.; Zhang, Z.; Liang, Q.; Gao, F.; Yi, F.; Ma, M.; Liao, Q.; Kang, Z.; Zhang, Y. Green Hybrid Power System Based on Triboelectric Nanogenerator for Wearable/Portable Electronics. *Nano Energy* **2019**, *55*, 151−163.

(5) Zhang, W.; Diao, D.; Sun, K.; Fan, X.; Wang, P. Study on Friction-Electrification Coupling in Sliding-Mode Triboelectric Nanogenerator. *Nano Energy* **2018**, *48*, 456−463.

(6) Fang, Y.; Zou, Y.; Xu, J.; Chen, G.; Zhou, Y.; Deng, W.; Zhao, X.; Roustaei, M.; Hsiai, T. K.; Chen, J. Ambulatory Cardiovascular Monitoring Via a Machine-Learning-Assisted Textile Triboelectric Sensor. *Adv. Mater.* **2021**, *33*, No. 2104178.

(7) Wang, L.; Liu, Y.; Liu, Q.; Zhu, Y.; Wang, H.; Xie, Z.; Yu, X.; Zi, Y. A Metal-Electrode-Free, Fully Integrated, Soft Triboelectric Sensor Array for Self-Powered Tactile Sensing. *Microsyst. Nanoeng.* **2020**, *6*, 1−9.

(8) Pu, X.; Guo, H.; Tang, Q.; Chen, J.; Feng, L.; Liu, G.; Wang, X.; Xi, Y.; Hu, C.; Wang, Z. L. Rotation Sensing and Gesture Control of a Robot Joint via Triboelectric Quantization Sensor. *Nano Energy* **2018**, *54*, 453−460.

(9) Yang, J.; Chen, J.; Su, Y.; Jing, Q.; Li, Z.; Yi, F.; Wen, X.; Wang, Z.; Wang, Z. L. Eardrum-Inspired Active Sensors for Self-Powered

Cardiovascular System Characterization and Throat-Attached Anti-Interference Voice Recognition. *Adv. Mater.* **2015**, *27*, 1316−1326.

(10) Yi, F.; Zhang, Z.; Kang, Z.; Liao, Q.; Zhang, Y. Recent Advances in Triboelectric Nanogenerator-Based Health Monitoring. *Adv. Funct. Mater.* **2019**, *29*, No. 1808849.

(11) Luo, J.; Gao, W.; Wang, Z. L. The Triboelectric Nanogenerator as an Innovative Technology toward Intelligent Sports. *Adv. Mater.* **2021**, *33*, No. 2004178.

(12) Zhang, D.; Shi, J.; Si, Y.; Li, T. Multi-Grating Triboelectric Nanogenerator for Harvesting Low-Frequency Ocean Wave Energy. *Nano Energy* **2019**, *61*, 132−140.

(13) Zhang, W.; Gu, G.; Qin, H.; Li, S.; Shang, W.; Wang, T.; Zhang, B.; Cui, P.; Guo, J.; Yang, F.; Cheng, G.; Du, Z. Measuring the Actual Voltage of a Triboelectric Nanogenerator Using the Non-Grounded Method. *Nano Energy* **2020**, *77*, No. 105108.

(14) Hu, Y.; Wang, X.; Li, H.; Li, H.; Li, Z. Effect of Humidity on Tribological Properties and Electrification Performance of Sliding-Mode Triboelectric Nanogenerator. *Nano Energy* **2020**, *71*, No. 104640.

(15) Lee, Y.; Kim, W.; Bhatia, D.; Hwang, H. J.; Lee, S.; Choi, D. Cam-Based Sustainable Triboelectric Nanogenerators with a Resolution-Free 3D-Printed System. *Nano Energy* **2017**, *38*, 326−334.

(16) He, W.; Sohn, M.; Ma, R.; Kang, D. J. Flexible Single-Electrode Triboelectric Nanogenerators with MXene/PDMS Composite Film for Biomechanical Motion Sensors. *Nano Energy* **2020**, *78*, No. 105383.

(17) Matsunaga, M.; Hirotani, J.; Kishimoto, S.; Ohno, Y. High-Output, Transparent, Stretchable Triboelectric Nanogenerator Based on Carbon Nanotube Thin Film toward Wearable Energy Harvesters. *Nano Energy* **2020**, *67*, No. 104297.

(18) Kim, S.; Gupta, M. K.; Lee, K. Y.; Sohn, A.; Kim, T. Y.; Shin, K.-S.; Kim, D.; Kim, S. K.; Lee, K. H.; Shin, H.-J.; Kim, D.-W.; Kim, S.-W. Transparent Flexible Graphene Triboelectric Nanogenerators. *Adv. Mater.* **2014**, *26*, 3918−3925.

(19) Sahu, M.; Vivekananthan, V.; Hajra, S.; Abisegapriyan, K. S.; Raj, N. P. M. J.; Kim, S.-J. Synergetic Enhancement of Energy Harvesting Performance in Triboelectric Nanogenerator Using Ferroelectric Polarization for Self-Powered IR Signaling and Body Activity Monitoring. *J. Mater. Chem. A* **2020**, *8*, 22257−22268.

(20) Cheon, S.; Kang, H.; Kim, H.; Son, Y.; Lee, J. Y.; Shin, H.-J.; Kim, S.-W.; Cho, J. H. High-Performance Triboelectric Nanogenerators Based on Electrospun Polyvinylidene Fluoride−Silver Nanowire Composite Nanofibers. *Adv. Funct. Mater.* **2018**, *28*, No. 1703778.

(21) Jiang, H.; Lei, H.; Wen, Z.; Shi, J.; Bao, D.; Chen, C.; Jiang, J.; Guan, Q.; Sun, X.; Lee, S.-T. Charge-Trapping-Blocking Layer for Enhanced Triboelectric Nanogenerators. *Nano Energy* **2020**, *75*, No. 105011.

(22) Khun, N. W.; Tan, A. W. Y.; Sun, W.; Liu, E. Wear and Corrosion Resistance of Thick Ti-6Al-4V Coating Deposited on Ti-6Al-4V Substrate via High-Pressure Cold Spray. *J. Therm. Spray Technol.* **2017**, *26*, 1393−1407.

(23) Hemeda, A. A.; Zhang, C.; Hu, X. Y.; Fukuda, D.; Cote, D.; Nault, I. M.; Nardi, A.; Champagne, V. K.; Ma, Y.; Palko, J. W. Particle-Based Simulation of Cold Spray: Influence of Oxide Layer on Impact Process. *Addit. Manuf.* **2021**, *37*, No. 101517.

(24) Kim, J. H.; Seo, S. Fabrication of an Imperceptible Liquid Metal Electrode for Triboelectric Nanogenerator Based on Gallium Alloys by Contact Printing. *Appl. Surf. Sci.* **2020**, *509*, No. 145353.

(25) Lee, J. P.; Lee, J. W.; Baik, J. M. The Progress of PVDF as a Functional Material for Triboelectric Nanogenerators and Self-Powered Sensors. *Micromachines* **2018**, *9*, 532.

(26) Zhang, R.; Olin, H. Material Choices for Triboelectric Nanogenerators: A Critical Review. *EcoMat* **2020**, *2*, No. e12062.

(27) Jang, S.; Kim, H.; Kim, Y.; Kang, B. J.; Oh, J. H. Honeycomb-like Nanofiber Based Triboelectric Nanogenerator Using Self-Assembled Electrospun Poly(Vinylidene Fluoride-Co-Trifluoroethylene) Nano-fibers. *Appl. Phys. Lett.* **2016**, *108*, 143901.

(28) Liao, M.-H.; Huang, H.-Y.; Chuang, C.-C. Cite As. *Appl. Phys. Lett.* **2017**, *110*, 153901.

(29) Yao, C.; Hernandez, A.; Yu, Y.; Cai, Z.; Wang, X. Triboelectric Nanogenerators and Power-Boards from Cellulose Nanofibrils and Recycled Materials. *Nano Energy* **2016**, *30*, 103−108.

(30) Khandelwal, G.; Prashanth, N.; Raj, M. J.; Kim, S.-J.; Khandelwal, G.; Maria, N. P.; Raj, J.; Kim, S.-J. Materials Beyond Conventional Triboelectric Series for Fabrication and Applications of Triboelectric Nanogenerators. *Adv. Energy Mater.* **2021**, *11*, No. 2101170.

(31) Liu, Y.; Sun, N.; Liu, J.; Wen, Z.; Sun, X.; Lee, S. T.; Sun, B. Integrating a Silicon Solar Cell with a Triboelectric Nanogenerator via a Mutual Electrode for Harvesting Energy from Sunlight and Raindrops. *ACS Nano* **2018**, *12*, 2893−2899.

(32) Tang, W.; Jiang, T.; Ru Fan, F.; Fang Yu, A.; Zhang, C.; Cao, X.; Lin Wang, Z.; Tang, W.; Jiang, T.; Fan, F. R.; Yu, A. F.; Zhang, C.; Cao, X.; Wang, Z. L. Liquid-Metal Electrode for High-Performance Triboelectric Nanogenerator at an Instantaneous Energy Conversion Efficiency of 70.6%. *Adv. Funct. Mater.* **2015**, *25*, 3718−3725.

(33) Cui, N.; Gu, L.; Lei, Y.; Liu, J.; Qin, Y.; Ma, X.; Hao, Y.; Wang, Z. L. Dynamic Behavior of the Triboelectric Charges and Structural Optimization of the Friction Layer for a Triboelectric Nanogenerator. *ACS Nano* **2016**, *10*, 6131−6138.

(34) Feng, Y.; Zheng, Y.; Zhang, G.; Wang, D.; Zhou, F.; Liu, W. A New Protocol toward High Output TENG with Polyimide as Charge Storage Layer. *Nano Energy* **2017**, *38*, 467−476.

(35) Kim, Y. W.; Lee, H. B.; Yoon, J.; Park, S. H. 3D Customized Triboelectric Nanogenerator with High Performance Achieved via Charge-Trapping Effect and Strain-Mismatching Friction. *Nano Energy* **2022**, *95*, No. 107051.

(36) Assadi, H.; Kreye, H.; Gärtner, F.; Klassen, T. Cold Spraying − A Materials Perspective. *Acta Mater.* **2016**, *116*, 382−407.

(37) Yin, S.; Meyer, M.; Li, W.; Liao, H.; Lupoi, R. Gas Flow, Particle Acceleration, and Heat Transfer in Cold Spray: A Review. *J. Therm. Spray Technol.* **2016**, 874.

(38) An, S.; Joshi, B.; Yarin, A. L.; Swihart, M. T.; Yoon, S. S. Supersonic Cold Spraying for Energy and Environmental Applications: One-Step Scalable Coating Technology for Advanced Micro- and Nanotextured Materials. *Adv. Mater.* **2020**, No. 1905028.

(39) Viscusi, A.; Astarita, A.; della Gatta, R.; Rubino, F. A Perspective Review on the Bonding Mechanisms in Cold Gas Dynamic Spray. *Surf. Eng.* **2019**, *35*, 743−771.

(40) Liberati, A. C.; Che, H.; Vo, P.; Yue, S. Observation of an Indirect Deposition Effect While Cold Spraying Sn-Al Mixed Powders onto Carbon Fiber Reinforced Polymers. *J. Therm. Spray Technol.* **2020**, *29*, 134.

(41) Zou, H.; Guo, L.; Xue, H.; Zhang, Y.; Shen, X.; Liu, X.; Wang, P.; He, X.; Dai, G.; Jiang, P.; Zheng, H.; Zhang, B.; Xu, C.; Wang, Z. Quantifying and Understanding the Triboelectric Series of Inorganic Non-Metallic Materials. *Nat. Commun.* **2020**, *11*, 2093.

(42) Moridi, A.; Hassani-Gangaraj, S. M.; Guagliano, M.; Dao, M. Cold Spray Coating: Review of Material Systems and Future Perspectives. *Surf. Eng.* **2014**, *30*, 369.

(43) Winnicki, M.; Baszczuk, A.; Rutkowska-Gorczyca, M.; Małachowska, A.; Ambroziak, A. Corrosion Resistance of Tin Coatings Deposited by Cold Spraying. *Surf. Eng.* **2016**, *32*, 691.

(44) Huang, J.; Fu, X.; Liu, G.; Xu, S.; Li, X.; Zhang, C.; Jiang, L. Micro/Nano-Structures-Enhanced Triboelectric Nanogenerators by Femtosecond Laser Direct Writing. *Nano Energy* **2019**, *62*, 638−644.

(45) Fan, B.; Liu, G.; Fu, X.; Wang, Z.; Zhang, Z.; Zhang, C. Composite Film with Hollow Hierarchical Silica/Perfluoropolyether Filler and Surface Etching for Performance Enhanced Triboelectric Nanogenerators. *Chem. Eng. J.* **2022**, *446*, No. 137263.

(46) Kang, X.; Pan, C.; Chen, Y.; Pu, X. Boosting Performances of Triboelectric Nanogenerators by Optimizing Dielectric Properties and Thickness of Electrification Layer. *RSC Adv.* **2020**, *10*, 17752−17759.

(47) Elbanna, M. A.; Arafa, M. H.; Bowen, C. R. Experimental and Analytical Investigation of the Response of a Triboelectric Generator Under Different Operating Conditions. *Energy Technol.* **2020**, *8*, No. 2000576.

(48) Mariello, M.; Scarpa, E.; Algieri, L.; Guido, F.; Mastronardi, V. M.; Qualtieri, A.; de Vittorio, M. Novel Flexible Triboelectric

Nanogenerator Based on Metallized Porous PDMS and Parylene C. *Energies* **2020**, *13*, 1625.

(49) Zhang, Z.; Bai, Y.; Xu, L.; Zhao, M.; Shi, M.; Wang, Z. L.; Lu, X. Triboelectric Nanogenerators with Simultaneous Outputs in Both Single-Electrode Mode and Freestanding-Triboelectric-Layer Mode. *Nano Energy* **2019**, *66*, No. 104169.

(50) Yang, W.; Wang, X.; Li, H.; Wu, J.; Hu, Y.; Li, Z.; Liu, H. Fundamental Research on the Effective Contact Area of Micro-/Nano-Textured Surface in Triboelectric Nanogenerator. *Nano Energy* **2019**, *57*, 41−47.

(51) Luo, J.; Wang, Z.; Xu, L.; Wang, A. C.; Han, K.; Jiang, T.; Lai, Q.; Bai, Y.; Tang, W.; Fan, F. R.; Wang, Z. L. Flexible and Durable Wood-Based Triboelectric Nanogenerators for Self-Powered Sensing in Athletic Big Data Analytics. *Nat. Commun.* **2019**, *10*, 5147.

(52) Shi, Q.; Wang, H.; Wu, H.; Lee, C. Self-Powered Triboelectric Nanogenerator Buoy Ball for Applications Ranging from Environment Monitoring to Water Wave Energy Farm. *Nano Energy* **2017**, *40*, 203−213.

(53) Bunriw, W.; Harnchana, V.; Chanthad, C.; Huynh, V. N. Natural Rubber-TiO$_2$ Nanocomposite Film for Triboelectric Nanogenerator Application. *Polymer* **2021**, *13*, 2213.

(54) Wang, Z. L. Triboelectric Nanogenerators as New Energy Technology for Self-Powered Systems and as Active Mechanical and Chemical Sensors. 2013, *7*, 9533, DOI: 10.1021/nn404614z.

(55) Zhang, J.-H.; Hao, X. Enhancing Output Performances and Output Retention Rates of Triboelectric Nanogenerators via a Design of Composite Inner-Layers with Coupling Effect and Self-Assembled Outer-Layers with Superhydrophobicity. *Nano Energy* **2020**, *76*, No. 105074.

(56) Khan, S. A.; Zhang, H. L.; Xie, Y.; Gao, M.; Shah, M. A.; Qadir, A.; Lin, Y. Flexible Triboelectric Nanogenerator Based on Carbon Nanotubes for Self-Powered Weighing. *Adv. Eng. Mater.* **2017**, *19*, No. 1600710.

(57) Shi, X.; Zhang, S.; Gong, S. A Self-Powered and Arch-Structured Triboelectric Nanogenerator for Portable Electronics and Human-Machine Communication. *J. Mater. Chem. A* **2020**, *8*, 8997−9005.

(58) Zhang, J.; Feng, J.; Jia, L.; Zhang, H.; Zhang, G.; Sun, S.; Zhou, T. Laser-Induced Selective Metallization on Polymer Substrates Using Organocopper for Portable Electronics. 2019, 13714, DOI: 10.1021/acsami.9b01856.

(59) Chang, T.; Akin, S.; Kim, M. K.; Murray, L.; Kim, B.; Cho, S.; Huh, S.; Teke, S.; Couetil, L.; Jun, M. B. G.; Lee, C. H. A Programmable Dual-Regime Spray for Large-Scale and Custom-Designed Electronic Textiles. *Adv. Mater.* **2022**, *34*, No. 2108021.